Volumetric locking in finite elements

on the relation between constraint ratio and locking behavior

Bachelor Final Project

Bart Vossen

MT 08.31

July 31, 2008

Supervisors:
H. R. Javani Joni, MSc
dr. ir. R.H.J. Peerlings

Eindhoven University of Technology
Department of Mechanical Engineering
Division of Mechanics of Materials

Contents

1 Introduction **3**

2 Element formulations **4**

2.1 Governing equations 4

2.2 Displacement formulation 4

2.2.1 Full integration 6

2.2.2 Reduced integration 6

2.2.3 Constant dilatation 6

2.3 Herrmann Formulation 7

2.3.1 U-P-B formulation 9

2.4 Overview of element formulations 11

3 Constraint ratio **12**

3.1 Displacement formulation 13

3.2 Herrmann formulation 13

3.3 Special arrangements of elements 13

3.4 Constraint ratio for idealised mesh 14

3.5 Constraint ratio for arbitrary mesh 15

4 Numerical tests **17**

4.1 Cook's membrane 17

4.2 Thick cylinder 19

5 Conclusion **22**

A Strain distributions **23**

A.1 Bilinear displacement quadrilateral 23

A.2 Quadratic displacement quadrilateral 23

A.3 Linear displacement triangle 24
A.4 Quadratic displacement triangle 24
A.5 Linear displacement triangle enriched with bubble 24

Chapter 1

Introduction

During the forming of metals, plasticity occurs. For almost all metals, there is no volume change due to plastic deformation. In simulations of metal forming, the finite element method is often used. Using the standard finite element method to describe incompressible material behavior may cause numerical problems and/or lead to erroneous solutions due to locking, see for example [1, 5]. Locking may be caused by the fact that there are too many incompressibility constraints imposed on the discretized solution, relative to the number of degrees of freedom in this solution.

While the underlying goal of this project is incompressible plastic deformation in forming, we limit ourselves to incompressible or slightly compressible elastic materials in this report. Furthermore this report will focus on two dimensional problems, however, the extension to three dimensions can easily be made. The goal of this project is to investigate whether the ratio between the number of degrees of freedom and the number of incompressibility constraints imposed on the solution is predictive for the performance of elements in the incompressible limit.

First, several solutions to locking, as proposed in the literature [7, 2], are described. Since not all of these methods can be used for fully incompressible material, this project mainly focuses on slightly compressible material. However, for the relevant methods, also the fully incompressible case is considered. In all methods, both quadrilateral and triangular elements are considered.

Next, for each of these methods the constraint ratio, i.e. the ratio between number of degrees of freedom and incompressibility constraints, is calculated. This is done first for an idealised mesh and finally for some numerical examples. In these examples the value of the constraint ratio is compared with the accuracy of the solution obtained with the corresponding element. These numerical tests are performed using the finite element package MSC Marc.

Chapter 2

Element formulations

2.1 Governing equations

The equation which governs the deformation of the linear elastic material that is considered in this study, as well as other types of material, is the equilibrium equation

$$\vec{\nabla} \cdot \boldsymbol{\sigma} = \vec{0} \tag{2.1}$$

where $\boldsymbol{\sigma}$ is the second order stress tensor and body forces and the dependence on the coordinate $\vec{x}$ have been omitted for clarity.

The constitutive equation that relates stress and strain for linear elastic material may be written as

$$\boldsymbol{\sigma} = {}^4\boldsymbol{C} : \boldsymbol{\epsilon} \tag{2.2}$$

where ${}^4\boldsymbol{C}$ is a fourth order elasticity tensor and $\boldsymbol{\epsilon}$ is the strain tensor given by

$$\boldsymbol{\epsilon} = \frac{1}{2}(\vec{\nabla}\vec{u} + (\vec{\nabla}\vec{u})^T) \tag{2.3}$$

where $\vec{u}$ is the displacement field.

2.2 Displacement formulation

In the compressible case, the fourth order elasticity tensor ${}^4\boldsymbol{C}$ is written as

$${}^4\boldsymbol{C} = \kappa \boldsymbol{I}\boldsymbol{I} + 2G({}^4\boldsymbol{I}^S - \frac{1}{3}\boldsymbol{I}\boldsymbol{I}) \tag{2.4}$$

where κ is the bulk modulus, and G is the shear modulus of the material. From equations (2.2) and (2.4) we have

$$\boldsymbol{\sigma} = \kappa \mathrm{tr}(\boldsymbol{\epsilon})\boldsymbol{I} + 2G\boldsymbol{\epsilon}^d \tag{2.5}$$

It can be observed from equation (2.5) that if this form of the stress-strain relation were to be used to describe fully incompressible material behavior, i.e. for $\kappa = \infty$, the hydrostatic pressure, $p = -\kappa \mathrm{tr}(\boldsymbol{\epsilon})$, cannot be determined from the strain field anymore. This is because the

hydrostatic pressure is, in that case, not coupled to the volumetric deformation anymore. The Herrmann formulation, which is described in section 2.3, provides a solution for this case. For nearly incompressible material behavior however, the displacement formulation can be used. In this case κ is large, but finite. Because a material physically cannot sustain very high stresses, $\mathrm{tr}(\boldsymbol{\epsilon})$ must become very small for the stresses to be limited. Using the relation

$$\mathrm{tr}(\boldsymbol{\epsilon}) = \vec{\nabla} \cdot \vec{u} \tag{2.6}$$

it can be concluded that nearly incompressible material behavior imposes the following constraint on the solution:

$$\vec{\nabla} \cdot \vec{u} \approx 0 \tag{2.7}$$

The strong form of the elasticity problem, together with the boundary conditions, reads

$$\begin{aligned} \vec{\nabla} \cdot \boldsymbol{\sigma} &= \vec{0} \quad \text{in } V \\ \vec{u} &= \vec{u}^* \quad \text{on } S_u \\ \vec{t} = \vec{n} \cdot \boldsymbol{\sigma} &= \vec{t}^* \quad \text{on } S_t \end{aligned}$$

where $\boldsymbol{\sigma}$ is given by equation (2.5). The weak form of this problem is obtained by taking the scalar product with a vector test function $\vec{\phi}$, followed by integration on the domain V. Integration by parts and some reordering leads to the weak form

$$\int_V (\vec{\nabla}\vec{\phi})^T : {}^4\boldsymbol{C} : \vec{\nabla}\vec{u}\, dV = \int_S \vec{\phi} \cdot \vec{t}^* dS \tag{2.8}$$

Using the discrete domain V^h and the discrete boundary S^h as a replacement for the problem domain V and the boundary S respectively, the weak form can be discretized. To this end the displacement field $\vec{u}$ is replaced by a approximate field $\vec{u}^h$ of the form

$$\vec{u}^h = \underset{\sim}{N}^T \underset{\sim}{\vec{u}} \tag{2.9}$$

where $\underset{\sim}{\vec{u}}$ is a column containing nodal displacement values, and $\underset{\sim}{N}$ is a column containing shape functions. The test function $\vec{\phi}$ is similarly discretized as

$$\vec{\phi}^h = \underset{\sim}{N}^T \underset{\sim}{\vec{\phi}} \tag{2.10}$$

where $\underset{\sim}{\vec{\phi}}$ is a column containing the nodal values of $\vec{\phi}^h$. Using these discretizations and the fact that the result must hold for all $\underset{\sim}{\vec{\phi}}$, the weak form can be rewritten as

$$\int_{V^h} \vec{\nabla} N \cdot {}^4\boldsymbol{C} \cdot \vec{\nabla} N^T dV \cdot \underset{\sim}{\vec{u}} = \int_{S^h} \underset{\sim}{N} \vec{t}^* dS \tag{2.11}$$

Introducing the notation

$$\begin{aligned} \underset{\sim}{\underset{\sim}{\boldsymbol{K}}} &= \int_{V^h} \vec{\nabla} N \cdot {}^4\boldsymbol{C} \cdot \vec{\nabla} N^T dV \\ \underset{\sim}{\vec{t}} &= \int_{S^h} \underset{\sim}{N} \vec{t}^* dS \end{aligned}$$

equation (2.11) may be written as

$$\underline{\underline{\boldsymbol{K}}} \cdot \underset{\sim}{\vec{u}} = \underset{\sim}{\vec{t}} \tag{2.12}$$

To solve this system of equations, the matrix $\underline{\underline{\boldsymbol{K}}}$ and the column $\underset{\sim}{\vec{t}}$ should be known. Because analytically evaluating the integrals in the expressions for $\underline{\underline{\boldsymbol{K}}}$ and $\underset{\sim}{\vec{t}}$ is generally not possible, numerical integration is used. Besides the commonly used full integration scheme, there are several integration schemes that can be used to evaluate the integrals. In the next sections some integration schemes are briefly described, namely full integration, reduced integration and constant dilatation.

2.2.1 Full integration

For the full integration scheme, the number and the position of the integration points is chosen such that the integration is of an order that is high enough to preserve the rate of convergence which would result if exact integration were used [7]. As will be shown later, each integration point can give rise to an incompressibility constraint. Thus using more integration points means that more constraints may be applied to the solution.

2.2.2 Reduced integration

For slightly compressible materials, a possible way to solve locking is known as reduced integration. In reduced integration, the integrals in equation (2.11) are evaluated using fewer integration points than are required for full integration. This approach was initially based on purely heuristic arguments and the main reason for its success is associated with the fact that it provides the necessary singularity of the constraint part of the stiffness matrix, which avoids locking [7]. Since the stiffness matrix may become singular, the solution $\underset{\sim}{\vec{u}}$ has some entries that are not constrained, thus the finite element formulation may be able to give an appropriate solution to the problem that is solved. A disadvantage of the reduced integration scheme is that the stiffness matrix may become singular, thus leading to erroneous solutions, or no solution at all. For example, the element may deform without applying any force to it. This type of deformation is known as 'hourglassing', and should be avoided.

2.2.3 Constant dilatation

The constant dilatation method is based on a slight modification of the displacement formulation. In this approach, the fourth-order elasticity tensor ${}^4\boldsymbol{C}$, given by equation (2.4), is split into two parts, a volumetric part and a deviatoric part, according to

$${}^4\boldsymbol{C} = {}^4\boldsymbol{C}^v + {}^4\boldsymbol{C}^d \tag{2.13}$$

where the volumetric and deviatoric parts are given by

$${}^4\boldsymbol{C}^v = \kappa \boldsymbol{I}\boldsymbol{I} \tag{2.14}$$

$${}^4\boldsymbol{C}^d = 2G({}^4\boldsymbol{I}^S - \frac{1}{3}\boldsymbol{I}\boldsymbol{I}) \tag{2.15}$$

With this split, the stiffness matrix can be written as

$$\underline{\boldsymbol{K}} = \underline{\boldsymbol{K}}^v + \underline{\boldsymbol{K}}^d = \int_{V^h} \vec{\nabla} N \cdot {}^4\boldsymbol{C}^v \cdot \vec{\nabla} N^T dV + \int_{V^h} \vec{\nabla} N \cdot {}^4\boldsymbol{C}^d \cdot \vec{\nabla} N^T dV \tag{2.16}$$

It can be observed that $\underline{\boldsymbol{K}}^v$ is proportional to κ and $\underline{\boldsymbol{K}}^d$ is proportional to G. Since the ratio between κ and G approaches infinity for the nearly incompressible case, the numerical values in $\underline{\boldsymbol{K}}^v$ tend to be very large compared to those in $\underline{\boldsymbol{K}}^d$. Since it is the volumetric part of the stiffness matrix, $\underline{\boldsymbol{K}}^v$, that causes the volumetrically stiff behavior, special treatment of this term is required. As was shown in the previous section, reducing the order of integration leads to a reduction of the volumetrically stiff behavior. In contrast to the reduced integration scheme, in the constant dilatation approach, reduced integration is used only for the volumetric part of the stiffness matrix; the deviatoric part is integrated using full integration. The full integration of the deviatoric part leads to an advantage of the constant dilatation integration scheme, compared to the reduced integration scheme. For constant dilatation integration the stiffness matrix retains the correct rank, and therefore no hourglassing occurs. The use of more integration points does however come at a slightly higher cost in terms of computing time. Full equivalence of the constant dilatation method with the Herrmann formulation was shown to exist and this method was proven to work. The equivalence theorem, however, is beyond the scope of this project and will not be further discussed. More information on it can be found in [3].

2.3 Herrmann Formulation

As was mentioned in section 2.2, for fully incompressible material the displacement formulation cannot be used. Therefore it is necessary to have an alternative formulation for the stress-strain relation. In this alternative formulation the constitutive equation is written as

$$\boldsymbol{\sigma} = -p\boldsymbol{I} + 2G\boldsymbol{\epsilon}^d = -p\boldsymbol{I} + {}^4\boldsymbol{C}^d : \boldsymbol{\epsilon}^d \tag{2.17}$$

where the tensor ${}^4\boldsymbol{C}^d$ is given by equation (2.15) and p is the hydrostatic pressure. The pressure must be determined as part of the solution to the boundary-value problem and thus represents an additional unknown. Therefore an additional equation is necessary to have a well-posed system of equations. This equation is the kinematic condition of incompressibility

$$\vec{\nabla} \cdot \vec{u} = 0 \tag{2.18}$$

Now, equations (2.17) and (2.18) combined with the boundary conditions describe the fully incompressible case.

Since in this study also compressible and slightly compressible materials are considered, an extension of the above incompressible formulation should be used. To this end the constraint equation is rewritten in a form that can be used for compressible, slightly compressible, and incompressible materials as follows

$$\vec{\nabla} \cdot \vec{u} + \frac{p}{\kappa} = 0 \tag{2.19}$$

In the fully incompressible case ($\kappa = \infty$), equation (2.19) becomes the incompressibility condition (2.18) and p is the independent hydrostatic pressure. If the material is (slightly) compressible,

p may be eliminated from equation (2.17) by way of (2.19) to obtain the constitutive equation of the compressible case, equation (2.5).

Combining the above constitutive equations with boundary conditions leads to the strong form of the boundary-value problem, where the body forces have been omitted for simplicity.

$$\begin{aligned} \vec{\nabla} \cdot \boldsymbol{\sigma} &= \vec{0} \quad \text{in } V \\ \vec{\nabla} \cdot \vec{u} + \frac{p}{\kappa} &= 0 \quad \text{in } V \\ \vec{u} &= \vec{u}^* \quad \text{on } S_u \\ \vec{t} = \vec{n} \cdot \boldsymbol{\sigma} &= \vec{t}^* \quad \text{on } S_t \end{aligned}$$

The weak form of this problem is obtained by taking the scalar product of the equilibrium equation with a vector test function $\vec{\phi}$ followed by integration on the domain V. An additional test function ψ is introduced to impose condition (2.19). The weak form can be found, after application of the divergence theorem and some reordering, to be

$$\int_V (\vec{\nabla}\vec{\phi})^T : {}^4\boldsymbol{C}^d : \vec{\nabla}\vec{u} dV - \int_V (\vec{\nabla} \cdot \vec{\phi}) p dV - \int_V \psi(\vec{\nabla} \cdot \vec{u} + \frac{p}{\kappa}) dV = \int_S \vec{\phi} \cdot \vec{t}^* dS \tag{2.20}$$

Using the discrete domain V^h and the discrete boundary S^h as a replacement for the problem domain V and the boundary S respectively, the weak form can be discretized. To this end the displacement field $\vec{u}$, and the pressure field p are replaced by the approximate fields $\vec{u}^h$ and p^h respectively. These approximate fields are of the form

$$\begin{aligned} \vec{u}^h &= \underset{\sim}{N}_u^T \vec{\underset{\sim}{u}} \\ p^h &= \underset{\sim}{N}_p^T \underset{\sim}{p} \end{aligned}$$

As can be seen from these equations, the displacement and pressure field both have their own set of shape functions. The discretizations of both fields need not be of the same order. An important property that can be observed from equation (2.20), is that the discretized pressure does not need to be continuous. This is because there are no derivatives of the pressure, or the pressure test function ψ, in the weak form of the problem.

The test functions are discretized in a similar way to the displacement and pressure fields:

$$\begin{aligned} \vec{\phi}^h &= \underset{\sim}{N}_u^T \vec{\underset{\sim}{\phi}} \\ \psi^h &= \underset{\sim}{N}_p^T \underset{\sim}{\psi} \end{aligned}$$

Using these discretizations and the fact that the result must hold for all $\vec{\underset{\sim}{\phi}}$ and $\underset{\sim}{\psi}$, the weak form can be rewritten as

$$\int_{V^h} \vec{\nabla} \underset{\sim}{N}_u \cdot {}^4\boldsymbol{C}^d \cdot (\vec{\nabla} \underset{\sim}{N}_u)^T dV \cdot \underset{\sim}{u} - \int_{V^h} \vec{\nabla} \underset{\sim}{N}_u \underset{\sim}{N}_p^T dV \underset{\sim}{p} = \int_{S^h} \underset{\sim}{N}_u \vec{t}^* dS \tag{2.21}$$

$$- \int_{V^h} \underset{\sim}{N}_p (\vec{\nabla} \underset{\sim}{N}_u)^T dV \cdot \underset{\sim}{u} - \int_{V^h} \frac{1}{\kappa} \underset{\sim}{N}_p \underset{\sim}{N}_p^T dV \underset{\sim}{p} = \underset{\sim}{0} \tag{2.22}$$

As was done for the displacement formulation in section (2.2), the following notation is introduced to allow the system to be written in a more compact form:

$$\begin{aligned}
\underline{\underline{\boldsymbol{K}}}_{uu} &= \int_{V^h} \vec{\nabla} \underset{\sim}{N}_u \cdot {}^4\boldsymbol{C}^d \cdot (\vec{\nabla} \underset{\sim}{N}_u)^T dV \\
\underline{\vec{K}}_{up} &= -\int_{V^h} \vec{\nabla} \underset{\sim}{N}_u \underset{\sim}{N}_p^T dV \\
\underline{K}_{pp} &= -\int_{V^h} \frac{1}{\kappa} \underset{\sim}{N}_p \underset{\sim}{N}_p^T dV \\
\vec{\underset{\sim}{t}} &= \int_{S^h} \underset{\sim}{N}_u \vec{t}^* dS
\end{aligned}$$

Using this notation, the system can be written as

$$\underline{\underline{\boldsymbol{K}}}_{uu} \cdot \vec{\underset{\sim}{u}} + \underline{\vec{K}}_{up} \underset{\sim}{p} = \vec{\underset{\sim}{t}} \tag{2.23}$$

$$\underline{\vec{K}}_{up}^T \cdot \vec{\underset{\sim}{u}} + \underline{K}_{pp} \underset{\sim}{p} = \underset{\sim}{0} \tag{2.24}$$

This system can be solved either simultaneously for both unknowns, or by eliminating one of the unknowns. If a discontinuous pressure interpolation is used for the analysis of compressible materials, the pressure degrees of freedom can be eliminated at the element level. Therefore, only operations on small matrices are involved in the elimination and the computational cost may be reduced significantly.

While the Herrmann formulation can be used in the fully incompressible case, locking may still occur in this formulation. The choice of the interpolations for the displacement and pressure play a crucial role in avoiding locking. Arbitrary combinations of displacement and pressure interpolations may prove to be ineffective in the incompressible case [2]. One way to possibly prevent locking in the Herrmann formulation, is to add an interior displacement node to the element, also known as a bubble function [7]. This bubble will be described in the next section.

2.3.1 U-P-B formulation

To give the element more freedom to deform, so as to satisfy the incompressibility condition whilst also giving a reasonable approximation to the solution of the problem that is being solved, an interior node is added to the element. With this bubble, the displacements are written as

$$\vec{u}^h = \underset{\sim}{N}_u^T \vec{\underset{\sim}{u}}_u + \underset{\sim}{N}_b^T \vec{\underset{\sim}{u}}_b \tag{2.25}$$

where $\underset{\sim}{N}_b$ is the column containing the bubble shape functions and $\vec{\underset{\sim}{u}}_b$ is the column containing the nodal values of the bubble displacement. The subscript u denotes the shape functions, displacement field, and test functions of the 'standard' element formulation. The test function is similarly written

$$\vec{\phi}^h = \underset{\sim}{N}_u^T \vec{\underset{\sim}{\phi}}_u + \underset{\sim}{N}_b^T \vec{\underset{\sim}{\phi}}_b \tag{2.26}$$

These discretizations can now be substituted in the weak form (2.20), to obtain

$$\int_V (\vec{\nabla}\vec{\phi})^T : {}^4\boldsymbol{C}^d : \vec{\nabla}\vec{u} dV = \int_{V^h} (\vec{\nabla}(\underset{\sim}{N}_u^T \vec{\underset{\sim}{\phi}}_u + \underset{\sim}{N}_b^T \vec{\underset{\sim}{\phi}}_b))^T : {}^4\boldsymbol{C}^d : \vec{\nabla}(\underset{\sim}{N}_u^T \vec{\underset{\sim}{u}}_u + \underset{\sim}{N}_b^T \vec{\underset{\sim}{u}}_b)) dV \tag{2.27}$$

$$\int_V (\vec{\nabla}\cdot\vec{\phi})p dV = \int_{V^h} (\vec{\nabla}\cdot(\underset{\sim}{N}_u^T\underset{\sim}{\vec{\phi}}_u + \underset{\sim}{N}_b^T\underset{\sim}{\vec{\phi}}_b))\underset{\sim}{N}_p^T\underset{\sim}{p}dV \tag{2.28}$$

$$\int_V \psi(\vec{\nabla}\cdot\vec{u} + \frac{p}{\kappa})dV = \int_{V^h} \underset{\sim}{N}_p^T\underset{\sim}{\psi}(\vec{\nabla}\cdot(\underset{\sim}{N}_u^T\underset{\sim}{\vec{u}}_u + \underset{\sim}{N}_b^T\underset{\sim}{\vec{u}}_b) + \frac{\underset{\sim}{N}_p^T\underset{\sim}{p}}{\kappa})dV \tag{2.29}$$

$$\int_S \vec{\phi}\cdot\vec{t}^*dS = \int_{S^h} (\underset{\sim}{N}_u^T\underset{\sim}{\vec{\phi}}_u + \underset{\sim}{N}_b^T\underset{\sim}{\vec{\phi}}_b)\cdot\vec{t}^*dS \tag{2.30}$$

By using orthogonality of spaces, and the fact that the bubble vanishes on the element edges, the following equations hold

$$\int_{V^h} (\vec{\nabla}\underset{\sim}{N}_u^T\underset{\sim}{\vec{\phi}}_u)^T : {}^4\boldsymbol{C}^d : \vec{\nabla}\underset{\sim}{N}_b^T\underset{\sim}{\vec{u}}_b dV = \int_{V^h} (\vec{\nabla}\underset{\sim}{N}_b^T\underset{\sim}{\vec{\phi}}_b)^T : {}^4\boldsymbol{C}^d : \vec{\nabla}\underset{\sim}{N}_u^T\underset{\sim}{\vec{u}}_u dV = \int_{S^h} \underset{\sim}{N}_b^T\underset{\sim}{\vec{\phi}}_b\cdot\vec{t}^*dS = 0 \tag{2.31}$$

Realising that the result should hold for all test functions, thus for all possible columns $\underset{\sim}{\vec{\phi}}_u$, $\underset{\sim}{\vec{\phi}}_b$, $\underset{\sim}{\psi}$ and seperating equations with different test functions, the system can be written as

$$\int_{V^h} \vec{\nabla}\underset{\sim}{N}_u\cdot{}^4\boldsymbol{C}^d\cdot(\vec{\nabla}\underset{\sim}{N}_u)^T dV\cdot\underset{\sim}{\vec{u}}_u - \int_{V^h} \vec{\nabla}\underset{\sim}{N}_u\underset{\sim}{N}_p^T dV\underset{\sim}{p} = \int_{S^h} \underset{\sim}{N}_u\vec{t}^*dS \tag{2.32}$$

$$\int_{V^h} \vec{\nabla}\underset{\sim}{N}_b\cdot{}^4\boldsymbol{C}^d\cdot(\vec{\nabla}\underset{\sim}{N}_b)^T dV\cdot\underset{\sim}{\vec{u}}_b - \int_{V^h} \vec{\nabla}\underset{\sim}{N}_b\underset{\sim}{N}_p^T dV\underset{\sim}{p} = \underset{\sim}{\vec{0}} \tag{2.33}$$

$$-\int_{V^h} \underset{\sim}{N}_p(\vec{\nabla}\underset{\sim}{N}_u)^T dV\cdot\underset{\sim}{\vec{u}}_u - \int_{V^h} \underset{\sim}{N}_p(\vec{\nabla}\underset{\sim}{N}_b)^T dV\cdot\underset{\sim}{\vec{u}}_b - \int_{V^h} \frac{1}{\kappa}\underset{\sim}{N}_p\underset{\sim}{N}_p^T dV\underset{\sim}{p} = \underset{\sim}{0} \tag{2.34}$$

In addition to the notation that was introduced in section 2.3, the following definitions are introduced to write the equations in a more compact form

$$\begin{aligned}\underline{\boldsymbol{K}}_{bb} &= \int_{V^h} \vec{\nabla}\underset{\sim}{N}_b\cdot{}^4\boldsymbol{C}^d\cdot(\vec{\nabla}\underset{\sim}{N}_b)^T dV\\ \underline{\vec{K}}_{bp} &= \int_{V^h} \vec{\nabla}\underset{\sim}{N}_b\underset{\sim}{N}_p^T dV\end{aligned}$$

The system can now be written as

$$\underline{\boldsymbol{K}}_{uu}\cdot\underset{\sim}{\vec{u}}_u + \underline{\vec{K}}_{up}\underset{\sim}{p} = \underset{\sim}{\vec{t}} \tag{2.35}$$

$$\underline{\boldsymbol{K}}_{bb}\cdot\underset{\sim}{\vec{u}}_b - \underline{\vec{K}}_{bp}\underset{\sim}{p} = \underset{\sim}{\vec{0}} \tag{2.36}$$

$$\underline{\vec{K}}_{up}^T\cdot\underset{\sim}{\vec{u}}_u - \underline{\vec{K}}_{bp}^T\cdot\underset{\sim}{\vec{u}}_b + \underline{K}_{pp}\underset{\sim}{p} = \underset{\sim}{0} \tag{2.37}$$

The bubble displacement can be eliminated from the system by way of equation (2.36) to obtain

$$\underset{\sim}{\vec{u}}_b = \underline{\boldsymbol{K}}_{bb}^{-1}\cdot\underline{\vec{K}}_{bp}\underset{\sim}{p} \tag{2.38}$$

Because this elimination can be performed elementwise, the bubble does not add significantly to the computational cost of the system. It does, however, require a higher order of integration.

2.4 Overview of element formulations

In the previous sections the finite element formulations have been described in general terms. In this section the precise elements that are used in the analysis in this report are listed. Figures 2.1 and 2.2 show the quadrilateral and triangular elements respectively, with the position of the displacement nodes, pressure nodes, and integration points indicated. In figure 2.2(d) the legend is given. For the constant dilatation element, the full integration scheme, figure 2.1(a), is used on the deviatoric part of the stiffness matrix, and the recuded integration scheme, figure 2.1(b), is used on the volumetric part of the stiffness matrix. For the Herrmann elements, the position and number of the integration points is not listed. For these elements, the order of integration is always chosen in a way that the integration is accurate enough to be of no influence on the results.

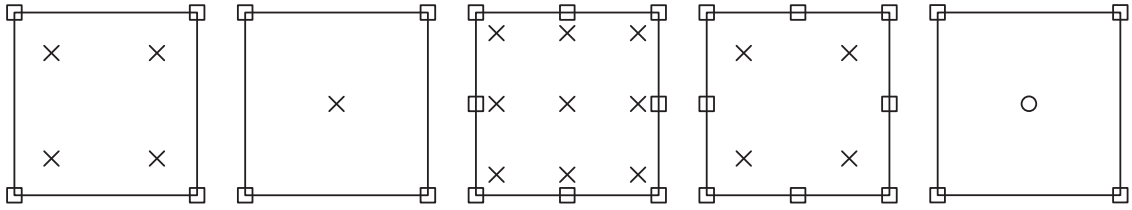

(a) Q1FI (b) Q1RI (c) Q2FI (d) Q2RI (e) Q1P0

Figure 2.1: Quadrilateral elements

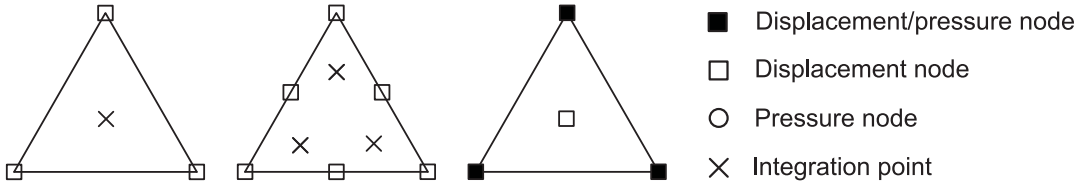

(a) T1 (b) T2 (c) T1P1B0 (d) Legend

Figure 2.2: Triangular elements and legend

Chapter 3

Constraint ratio

In discretizing the solution $\vec{u}^h$, p^h, a finite number of degrees of freedom is introduced instead of the continuous fields $\vec{u}$ and p. For an incompressible material, also a number of incompressibility constraints are imposed on the solution. What happens in locking is that the finite element method is not able anymore to give a reasonable approximation to the solution of the problem while also meeting the incompressibility condition. Too many constraints are imposed on the solution, compared to the number of degrees of freedom of this solution. Therefore, the ratio between number of degrees of freedom in the solution and the number of constraints imposed on it is an indicator for the element performance. However, it should be noted that this method is not a precise mathematical method for assessing elements but rather a quick and simple tool for obtaining an indication of element performance.

The constraint ratio r is defined by

$$r \equiv \frac{n_{dof}}{n_c} \tag{3.1}$$

where n_{dof} is the number of degrees of freedom, and n_c is the number of incompressibility constraints. Ideally r should equal the value obtained for the continuum problem. For a $2D$ continuum problem, $n_{dof} = 2$ and the incompressibility constraint (2.18) gives rise to one constraint, i.e. $n_c = 1$. This means that in two dimensions the optimum value of r should be 2. A value of r much greater than 2 indicates that not enough incompressibility conditions are present, so the incompressibility condition may be poorly approximated. A value of r less than 2 indicates a tendency to lock. For values of $r \leq 1$ there are more constraints than there are degrees of freedom; in this case, severe locking is expected.

An important limitation of the constraint ratio arises for elements with the same interpolation for the pressure as for the displacement. Although these elements often have a constraint ratio of 2, the ideal value, they show spuriour pressure modes and are generally a poor choice for (nearly) incompressible analysis.

The method to calculate the number of volumetric constraints is different for the Herrmann formulation and for the displacement formulation. In the next sections it will be explained how to calculate the constraint ratio for both element formulations. It should be mentioned that the maximum number of volumetric constraints is given by the total number of independent volumetric strain distributions in the entire mesh, because if all volumetric strain distributions are constrained to be zero, incompressibility is attained. Adding more constraint equations does not increase the number of actual volumetric constraints, because the extra constraints will be

linearly dependent.

3.1 Displacement formulation

For the standard displacement formulation nearly incompressible material behavior is enforced by the material law, resulting in the constraint given by equation (2.7). As was mentioned in section 2.2, fully incompressible material cannot be described with the displacement formulation. Since the constraints are imposed in a strong form in the displacement formulation, the number of constraints depends on the number of quadrature points, as these are the only locations where the constraints have to be fulfilled. If a constraint is violated elsewhere in the mesh, the finite element discretization cannot 'see' this. If fewer quadrature points are used, the elements become less stiff. This explains why reduced integration is a possible solution to volumetric locking. However, in reduced integration the risk of hourglassing is a disadvantage.

In case of full or reduced integration, the number of volumetric constraints is given by the minimum of the number of independent volumetric strain distributions and the number of quadrature points used to evaluate the stiffness matrix. For the constant dilatation integration scheme there are two terms in the stiffness matrix, a volumetric part and a deviatoric part. In this case the number of quadrature points used to evaluate the volumetric part is relevant, because this is the part that enforces the volumetrically stiff behavior.

3.2 Herrmann formulation

The incompressibility condition for the Herrmann formulation is given by equation (2.19). The weak form of this condition is given by equation (2.20). So, in the Herrmann formulation the incompressibility condition is applied in a weak sense. As long as the incompressibility conditions arising from equation (2.20) are linearly independent, the number of constraints equals the number of pressure equations, i.e. the number of pressure nodes. However, if there are more pressure weighting functions, and consequently incompressibility conditions, than there are independent volumetric strain distributions, the incompressibility conditions are linearly dependent. In this case, the number of constraints is given by the number of independent volumetric strain distributions.

3.3 Special arrangements of elements

To calculate the total number of volumetric constraints in the mesh, one may simply multiply the number of volumetric constraints per element by the total number of elements. This method however, does not always provide the correct result. For some special arrangements of elements, the total number of constraints may be less than this number. However, since it is necessary to combine a number of elements to eliminate one constraint, the improvement is small.

An arrangement of elements that is known to reduce the number of constraints is shown in figure 3.1. The linear triangular elements form a quadrilateral and its diagonals. This combination has the property that if the incompressibility constraint is satisfied in three of the elements, the

constraint in the fourth element is automatically satisfied. This property was found and proven by Nagtegaal *et al.* [4]. It also holds for quadratic triangular elements.

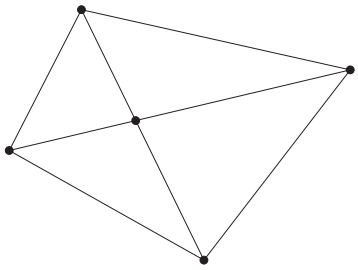

Figure 3.1: Arrangement with dependent constraints

3.4 Constraint ratio for idealised mesh

The constraint ratio can be readily calculated for a square, well structured, infinitely large mesh, of which a part is depicted in figures 3.2 and 3.3 for triangular and quadrilateral elements respectively. For this mesh, the number of volumetric strain distributions is equal to the number of volumetric strain distributions per element multiplied by the number of elements. In table 3.1 the number of volumetric strain distributions and the number of integration points and pressure nodes per element are given for the displacement formulation and Herrmann formulation respectively. In the last column of this table, the constraint ratios are shown. For further information on how the number of independent volumetric strain distributions is calculated for each element, see appendix A.

For both the displacement and Herrmann formulations, an example of how to calculate the constraint ratio is given below.

For the displacement formulation, the linear displacement triangular element is used. A part of the idealised mesh for this element is pictured in figure 3.2. For this element, we know that (see appendix A.3):

$$\vec{\nabla} \cdot \vec{u}^h = \beta_{1x} + \beta_{2y} \tag{3.2}$$

so there is one independent volumetric strain term available in $\vec{u}^h$. There is one integration point in the element, in which the constraint is applied. Thus, there is one constraint per element. From figure 3.2 it can be seen that each displacement node is shared by six elements, meaning that each element has a total of 3 times 1/6 displacement nodes. Since each displacement node represents two degrees of freedom, the element has one degree of freedom. The constraint ratio, therefore, is 1 / 1 = 1.

For the Herrmann formulation, the bilinear displacement, constant pressure element is used as an example. A part of the idealised mesh for this element is pictured in figure 3.3. For this element, we know that (see appendix A.1):

$$\vec{\nabla} \cdot \vec{u}^h = \beta_{1x} + \beta_{2y} + \beta_{3x}y + \beta_{3y}x \tag{3.3}$$

so there are three independent volumetric strain terms available in $\vec{u}^h$. There is, however, only one pressure node in the element, thus only one incompressibility constraint arises from the

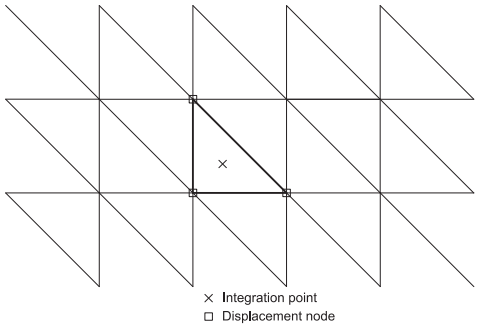

Figure 3.2: Part of the idealised mesh for triangular elements

weak form of the incompressibility condition. Furthermore, it can be determined that each element has two degrees of freedom, thus the constraint ratio is 2 / 1 = 2.

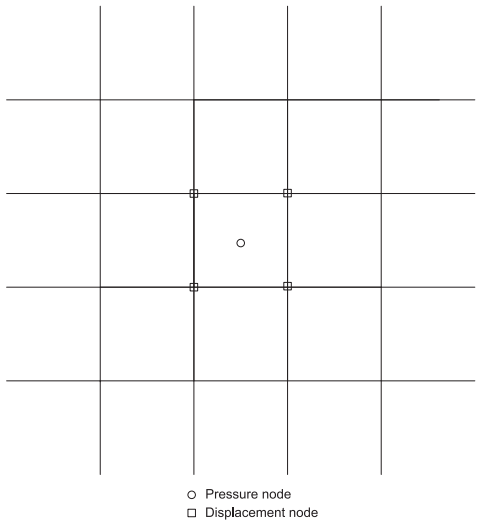

Figure 3.3: Part of the idealised mesh for quadrilateral elements

3.5 Constraint ratio for arbitrary mesh

The previous section considered the constraint ratio for a square, regular mesh. However, meshes generally are not square and regular, so it is necessary to be able to calculate the constraint ratio also for abitrary meshes. It can be observed from table 3.1 that for the Q1RI, Q1CD, Q1P0, Q2RI, and T1P1B0 elements the number of constrains is determined by the number of integration points for the displacement formulation and the number of pressure nodes for the Herrmann formulation. For these elements, it is assumed that, even for an arbitrary mesh, the number of strain distributions will always be higher than the number of integration points or pressure nodes. This means that, for these elements, the number of constraints can be easily calculated by multiplying the number of integration points or pressure nodes per element by the number

Element	ndof	Strain distributions	Integration points	Pressure nodes	Constraint ratio
Q1FI	2	3	4		2/3
Q1RI	2	3	1		2
Q1CD	2	3	1		2
Q1P0	2	3		1	2
Q2FI	6	6	9		1
Q2RI	6	6	4		3/2
T1	1	1	1		1
T2	4	3	3		4/3
T1P1B0	3	3		1/2	6

Table 3.1: Constraint ratios for idealised mesh. Values on a per element basis

of elements.

For the Q1FI, Q2FI, T1, and T2 elements, the number of independent volumetric strain distributions determines the number of constraints per element. This means that in the calculation of the number of constraints, special arrangements of elements, as mentioned in section 3.3, are taken into account.

Chapter 4

Numerical tests

To examine the relation between the constraint ratio and the locking behavior, two numerical testcases have been considered. In these tests, the constraint ratio was calculated as described in section 3.5 for all element formulations listed in section 2.4. The error in the results of the finite element code was also calculated, and the absolute value of the relative error was plotted. This error is defined as

$$e = \frac{|u_r - u|}{|u|} \tag{4.1}$$

where u is a displacement characteristic of the exact solution, or the solution obtained with a very fine mesh for problems for which no analytical solution exists, and u_r is the solution obtained with the finite element method. To study the convergence upon mesh refinement, the meshes that are used in the tests are refined in each subsequent simulation. This refinement is done by keeping the structure of the mesh the same, whilst subdividing each element into more elements. The number of displacement degrees of freedom in the mesh is calulated by multiplying the number of displacement nodes by the number of space dimensions. The total number of degrees of freedom also takes into account the number of pressure degrees of freedom. For the Q1P0 element, each element has one pressure degree of freedom. For the T1P1B0 element, each displacement node is also a pressure node, except for the bubble node. For this element, the bubble node is condensed out of the element matrix before the assembly of the global matrix, so the bubble node does not add to the number of degrees of freedom. All simulations were performed using the finite element package MSC Marc with MSC Mentat as graphic front-end. In the next two sections, the two tests are explained in more detail.

4.1 Cook's membrane

The first test is known as Cook's membrane. This test consists in a tapered plate clamped on one of its sides and a transversal load applied to the opposite side. The plate deforms in plane strain and its dimensions and loading are shown in figure 4.1(a). The material parameters are: $E = 250$, $\nu = 0.4999$. This means that the ratio between the bulk modulus and shear modulus is $\kappa/G = 5 \cdot 10^3$. The vertical displacement of the plate's tip was calculated using the finite element method and the results are compared for all element formulations. For this test, there exists no analytical solution. Therefore, a solution was obtained with a very fine mesh (62500 Q1 constant

dilatation elements). Examples of the meshes that were used for quadrilateral and triangular elements are shown in figures 4.1(b) and 4.1(c) respectively. It should be noted that the structure of these meshes is the same for the finer and coarser meshes that were used in the simulations.

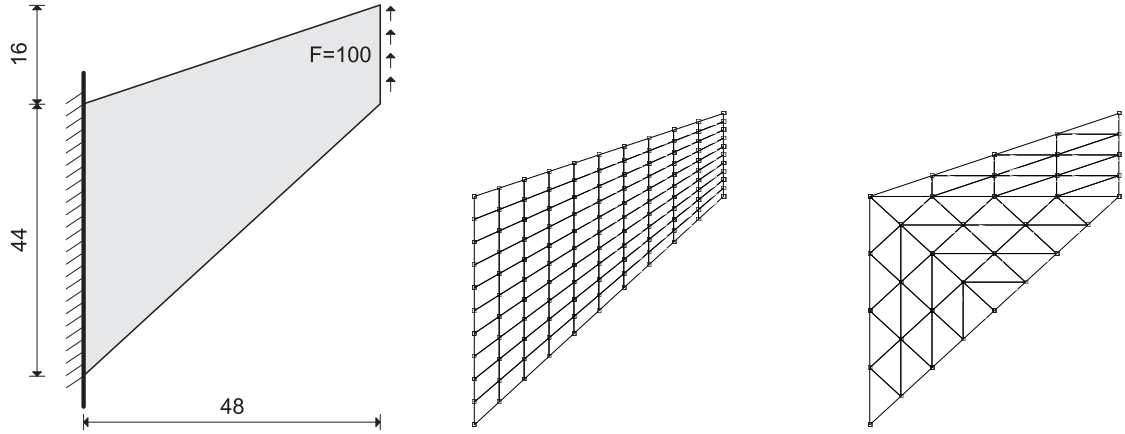

(a) Geometry and loads (b) Quadrilateral base mesh (c) Triangular base mesh

Figure 4.1: Cook's membrane.

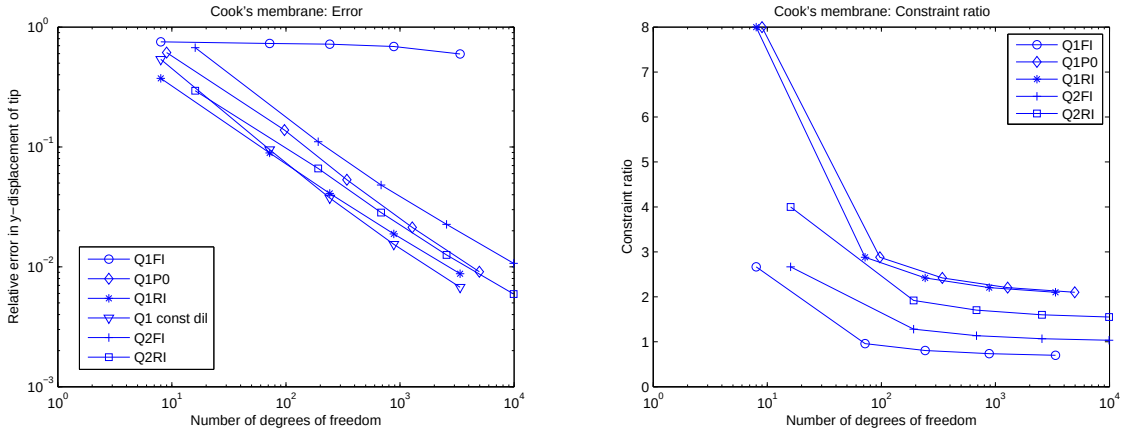

(a) Results (b) Constraint ratio

Figure 4.2: Cook's membrane. Quadrilateral elements

The results for the constant dilatation element (Q1CD) are exactly the same as for the reduced integration element (Q1RI) and are therefore not plotted.

It can be observed from figures 4.2(b) and 4.3(b) that the constraint ratios converge to the values listed in table 3.1 upon mesh refinement. This means that for fine meshes, the constraint ratio is predicted well by the idealised mesh. For the quadrilateral elements (figure 4.2(a)), it can be seen that the standard isoparametric element (Q1FI) performs poorly. This can also be seen from the constraint ratio, which is $2/3$, indicating severe locking. Furthermore, the quadratic full integration element (Q2FI), having a constraint ratio of 1, perform worse compared to the other formulations. The differences between the other element formulations are small. The best performing elements (Q1CD, Q1RI, and Q1P0) have a constraint ratio of 2. The Q2RI formulation

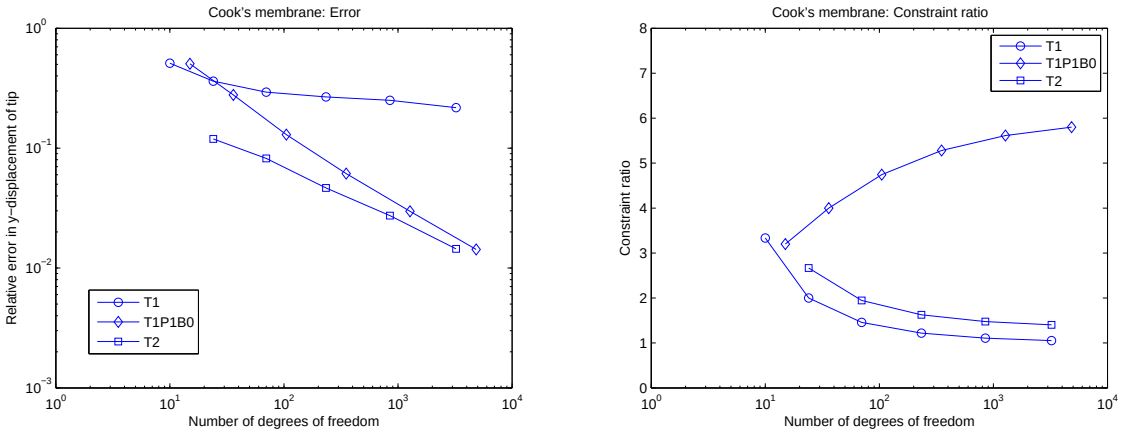

(a) Results

(b) Constraint ratio

Figure 4.3: Cook's membrane. Triangular elements

performs equally well, whilst having a slightly lower constraint ratio than the optimal value of 2.

For the triangular elements (figure 4.3(a)), the quadratic element (T2) and the bubble-enhanced triangle (T1P1B0) perform similarly well for fine meshes. Their constraint ratios however, differ significantly. The T2 elements have a constraint ratio of $4/3$, indicating a tendency for locking, and the T1P1B0 elements have a constraint ratio of 6, indicating a poor approximation of the incompressibility condition. The linear displacement triangle (T1) performs poorly. The constraint ratio for this element is 1. This element also shows spurious pressure modes, i.e. the 'checkerboard' pressure pattern. This behavior for this element was already mentioned by Zienkiewicz and Taylor [7].

From the results it can be concluded that a constraint ratio close to 2 indeed indicates a good element behavior. The lower the constraint ratio gets, the larger the larger the error and poorer the convergence. The results show that a constraint ratio lower than 1 indicates severe locking, as was stated in section 3. Furthermore, the T2 and T1P1B0 formulations both have a constraint ratio which is somewhat different from the optimal value of 2. The results are, however, quite similar, with both element formulations showing quite good performance. The good performance of the T1P1B0 element was not predicted by the constraint ratio, which is 6 for this element. Also no spurious pressure modes were observed in the results for this element.

4.2 Thick cylinder

The second test consists in a long, thick, elastic cylinder which is deformed due to the application of an internal pressure. The cylinder is in a plane strain state and its dimensions and loading are shown in figure 4.4(a). Because of the symmetry of the problem, only one quarter of the cylinder needs to be studied. The radial displacement of the exterior surface along the horizontal symmetry axis was calculated using the finite element method and the results are compared to the exact solution for all element formulations. The exact solution for the displacement at a distance

r from the axis of the cylinder is given by (see, for example [6]):

$$u(r) = p_i \frac{1+\nu}{E} \frac{r_i^2 r_e^2}{r_e^2 - r_i^2} \left(\frac{1}{r} + (1-2\nu)\frac{r}{r_e^2} \right) \tag{4.2}$$

where r_i, r_e are the internal and external radius of the cylinder respectively, p_i is the internal pressure, ν is the Poisson's ratio, and E is the Young's modulus. For the cylinder considered here, $E = 100, \nu = 0.4999$ and thus the ratio $\kappa/G = 5 \cdot 10^3$. The structure of the meshes that were used for quadrilateral and triangular elements is shown in figures 4.4(b) and 4.4(c) respectively. It may be noted that the triangular elements form exactly the special arrangement discussed in section 3.3.

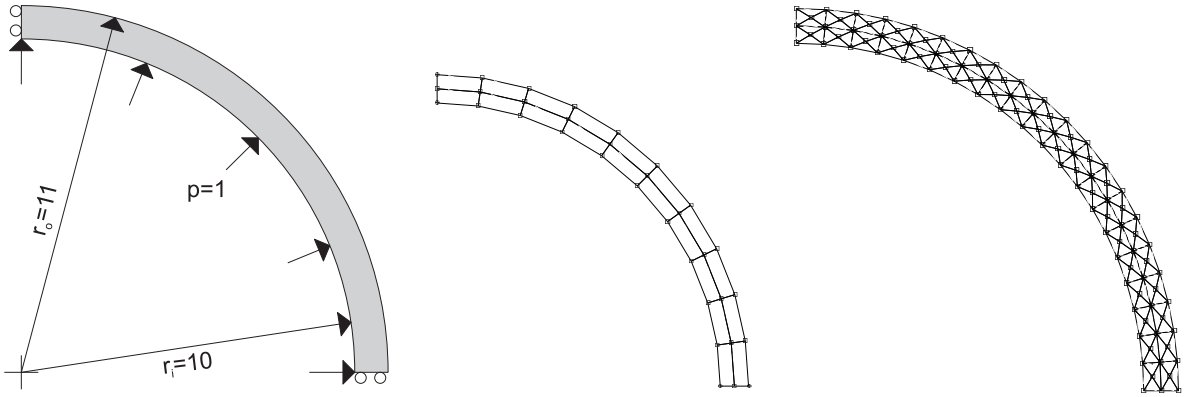

(a) Geometry and loads (b) Quadrilateral base mesh (c) Triangular base mesh

Figure 4.4: Thick cylinder under internal pressure.

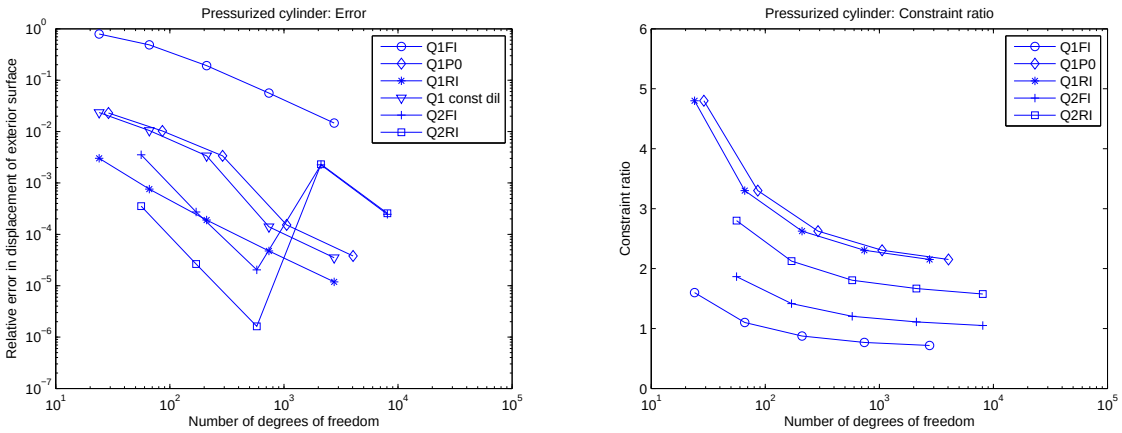

(a) Results (b) Constraint ratio

Figure 4.5: Pressurized cylinder. Quadrilateral elements

In the results of figure 4.5(a) the first thing that stands out is the behavior of the quadratic displacement elements (Q2FI and Q2RI). From a certain mesh density onwards, the finite element code overestimated the solution, so the error changes sign. The solution then nevertheless ap-

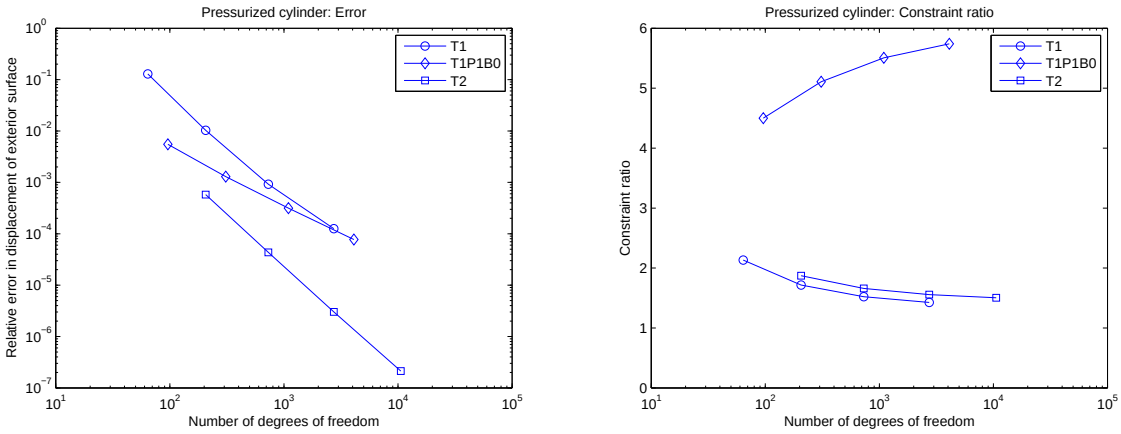

(a) Results

(b) Constraint ratio

Figure 4.6: Pressurized cylinder. Triangular elements

proaches the exact solution. This non-monotonic convergence may be caused by the structured mesh that was used for the test.

Again, it can be observed that the Q1FI element performs poorly. The elements that performed well in Cook's membrane, also perform well in this test. The Q1CD, Q1RI, and Q1P0 elements, having a constraint ratio of 2, outperform the quadratic displacement elements after the overestimation in the solution of the quadratic elements. Before the overestimation, the Q2RI performs significantly better than the Q2FI element. The Q2RI element has a constraint ratio that is closer to the optimal value, compared to the Q2FI element.

For the triangular elements, none of the elements performs dramatically poorly, compared to the other formulations. This may be related to the constraint ratio, which is for the displacement formulation elements (T1 and T2) higher than the value for the idealised mesh. This is caused by the special arrangement of elements that was used in the mesh for the cylinder. For the T1P1B0 elements, this special arrangement has no influence on the constraint ratio, because the number of constraints is, even for the special arrangement of elements, determined by the number of pressure nodes. This may also explain why both displacement formulation elements perform equally well compared to the T1P1B0 element. The T2 element performs better than the T1 element. It can be observed that the T2 element also has a constraint ratio that is closer to the optimal value. The T1 element however, again shows spurious pressure modes. Both the T2 and T1P1B0 elements do not suffer from these modes.

It may be concluded from these data that again elements with a constraint ratio lower than 1 perform poorly. Elements with a constraint ratio close to the optimal value perform well.

Chapter 5

Conclusion

The results presented in the previous chapter show that the constraint ratio is a good indicator for an element's sensitivity to volumetric locking. Locking can be expected for elements having a constraint ratio lower than 1. Also elements with a constraint ratio of 1 tend to perform poorly, however, the Q2FI element performed quite well in the pressurized cylinder test. This means that one should be careful in using these elements. Furthermore, the constraint ratio is no indicator for the presence of spurious pressure modes, as have been observed for the T1 element. The presence of spurious pressure modes is, however, a significant limitation of some elements.

To be able to come to a more precise relation between constraint ratio and volumetric locking behavior, it would be useful to perform more tests. What might especially be useful, is to redo the same tests with a more random mesh. For the tests that have been performed, the structure of the mesh may have been of a significant influence on the results. In 'real' simulations often automatically generated meshes are used, and these meshes in general are not as structured as the meshes that were used here.

Finally, if a choice for one element would have to be made, the Q1 constant dilatation element would be a good choice. This element performed well in both tests, and does not have the problem of hourglassing. It is, however, less flexible regarding automatic meshing, in which triangular elements are in favoured. The triangular element that would be a good choice is the T2 element. This element performs quite well in both tests and does not show spurious pressure modes.

Appendix A

Strain distributions

In this section, it is shown how the number of volumetric strain distributions is calculated for the square mesh. This calculation is done for all the elements that were used in the examples.

A.1 Bilinear displacement quadrilateral

For the bilinear displacement quadrilateral $\vec{u}^h$ can be written as

$$\underset{\sim}{u}^h = \begin{bmatrix} u_x^h \\ u_y^h \end{bmatrix} = \begin{bmatrix} \beta_{0x} + \beta_{1x}x + \beta_{2x}y + \beta_{3x}xy \\ \beta_{0y} + \beta_{1y}x + \beta_{2y}y + \beta_{3y}xy \end{bmatrix}$$

where β_{ij} are parameters which depend on the nodal values of $\vec{u}^h$ and the lengths of the element edges. It follows that

$$\vec{\nabla} \cdot \vec{u}^h = (\beta_{1x} + \beta_{2y})1 + \beta_{3x}y + \beta_{3y}x$$

so there are three independent volumetric strain terms available in $\vec{u}^h$.

A.2 Quadratic displacement quadrilateral

For the quadratic displacement quadrilateral $\vec{u}^h$ can be written as

$$\underset{\sim}{u}^h = \begin{bmatrix} u_x^h \\ u_y^h \end{bmatrix} = \begin{bmatrix} \beta_{0x} + \beta_{1x}x + \beta_{2x}y + \beta_{3x}xy + \beta_{4x}x^2 + \beta_{5x}y^2 + \beta_{6x}xy^2 + \beta_{7x}x^2y \\ \beta_{0y} + \beta_{1y}x + \beta_{2y}y + \beta_{3y}xy + \beta_{4y}x^2 + \beta_{5y}y^2 + \beta_{6y}xy^2 + \beta_{7y}x^2y \end{bmatrix}$$

It follows that

$$\vec{\nabla} \cdot \vec{u}^h = (\beta_{1x} + \beta_{2y})1 + (2\beta_{4x} + \beta_{3y})x + (\beta_{3x} + 2\beta_{5y})y + 2(\beta_{6y} + \beta_{7x})xy + \beta_{6x}y^2 + \beta_{7y}x^2$$

so there are six independent volumetric strain terms available in $\vec{u}^h$.

A.3 Linear displacement triangle

For the linear displacement triangle $\vec{u}^h$ can be written as

$$\underset{\sim}{u}^h = \begin{bmatrix} u_x^h \\ u_y^h \end{bmatrix} = \begin{bmatrix} \beta_{0x} + \beta_{1x}x + \beta_{2x}y \\ \beta_{0y} + \beta_{1y}x + \beta_{2y}y \end{bmatrix}$$

It follows that

$$\vec{\nabla} \cdot \vec{u}^h = (\beta_{1x} + \beta_{2y})1$$

so there is one independent volumetric strain terms available in $\vec{u}^h$

A.4 Quadratic displacement triangle

For the quadratic displacement triangle $\vec{u}^h$ can be written as

$$\underset{\sim}{u}^h = \begin{bmatrix} u_x^h \\ u_y^h \end{bmatrix} = \begin{bmatrix} \beta_{0x} + \beta_{1x}x + \beta_{2x}y + \beta_{3x}x^2 + \beta_{4x}y^2 + \beta_{5x}xy \\ \beta_{0y} + \beta_{1y}x + \beta_{2y}y + \beta_{3y}x^2 + \beta_{4y}y^2 + \beta_{5y}xy \end{bmatrix}$$

It follows that

$$\vec{\nabla} \cdot \vec{u}^h = (\beta_{1x} + \beta_{2y})1 + (2\beta_{3x} + \beta_{5y})x + (2\beta_{4y} + \beta_{5x})y$$

so there are three independent volumetric strain terms available in $\vec{u}^h$

A.5 Linear displacement triangle enriched with bubble

For the linear displacement triangle with bubble the bubble shape function is given by

$$N_b = 27xy(1 - x - y) \tag{A.1}$$

With this shape function $\vec{u}^h$ can be written as

$$\underset{\sim}{u}^h = \begin{bmatrix} u_x^h \\ u_y^h \end{bmatrix} = \begin{bmatrix} \beta_{0x} + \beta_{1x}x + \beta_{2x}y + \beta_{3x}(xy + x^2y + xy^2) \\ \beta_{0y} + \beta_{1y}x + \beta_{2y}y + \beta_{3y}(xy + x^2y + xy^2) \end{bmatrix}$$

It follows that

$$\vec{\nabla} \cdot \vec{u}^h = (\beta_{1x} + \beta_{2y})1 + \beta_{3x}(y + 2xy + y^2) + \beta_{3y}(x + 2xy + x^2)$$

so there are three independent volumetric strain terms available in $\vec{u}^h$

Bibliography

[1] Bell, R.W., Houlsby, G.T., Burd, H.J., 1993. Suitability of three-dimensional finite elements for modelling material incompressibility using exact integration. Communications in Numerical Methods in Engineering 9(4), 313-329.

[2] Hughes, T.J.R., 1987. The Finite Element Method, Prentice-Hall

[3] Malkus, D.S., Hughes, T.J.R., 1978. Mixed finite element methods - reduced and selective integration techniques: a unification of concepts. Computer methods in Applied Mechanics and Engineering 15(1), 63-81.

[4] Nagtegaal, J.C., Parks, D.M., Rice, J.R., 1974. On numerically accurate finite element solutions in the fully plastic range. Computer methods in Applied Mechanics and Engineering 4(2), 153-177.

[5] Oñate, E., Rojek, J., Taylor, R.L., Zienkiewicz, O.C., 2004. Finite calculus formulation for incompressible solids using linear triangles and tetrahedra. International Journal for Numerical Methods in Engineering 59(11), 1473-1500.

[6] Schreurs, P.J.G., 2007. Applied Elasticity in Engineering. Lecture notes.

[7] Zienkiewicz, O.C., Taylor, R.L., 2000. The Finite Element Method. 5th ed. Vol 1; Butterworth-Heinemann.